Friedel oscillations induced by non–magnetic impurities in the two–dimensional Hubbard model

W. Ziegler, H. Endres and W. Hanke

Institut für Theoretische Physik, Am Hubland, D-97074 Würzburg, Federal Republic of Germany

We study the interplay of correlations and disorder using an unrestricted Slave–Boson technique in real space. Within the saddle–point approximation, we find Friedel oscillations of the charge density in the vicinity of a nonmagnetic impurity, in agreement with numerical simulations. The corresponding amplitudes are suppressed by repulsive interactions, while attractive correlations lead to a charge–density–wave enhancement. In addition, we investigate the spatial dependence of the local magnetic moment and the formation of a magnetic state at the impurity site.

PACS numbers: 71.27.+a, 71.55.-i

I. INTRODUCTION

The combined effect of correlations and disorder, especially relevant in the context of high–T_c superconductors, poses the theoretical problem of consistently including both mechanisms in a formal approach[1–8]. The combined influence of disorder and many–body interactions can cause interesting new physical processes, and leads to unusual experimental properties. In addition to the drastic reduction of the transition temperature in cuprate superconductors, non–magnetic impurities can, for example, create local magnetic moments[9–15] which extend over up to several lattice spacings and enrich the phase diagram by introducing new disordered magnetic regions[16].

Electron density (Friedel) oscillations as a response to a local perturbation, i. e. the impurity, provides a clue to understanding the electronic properties (Fermi surface etc.) of a many–electron system. The period of the oscillation is determined by the Fermi surface, which may be defined by the singular points in the momentum distribution function. Especially in connection with the Fermi surface properties of high–temperature superconducting compounds[17] such as $Bi_2Sr_2CaCu_2O_{8+\delta}$, the Fermi surface evolution as a function of doping from the under–doped to maximally and over–doped regimes is an extremely important, yet unresolved issue[18]. A systematic study of Friedel oscillations, both in experiment and in the generic 2–D Hubbard model for the high–T_c cuprates, could, in principle, provide the required information on the Fermi surface and how it changes from the extremely–low doped case (with the possibility of "hole pockets", i. e. "small" Fermi surfaces) to the larger doped situation with a large Fermi surface, with the latter being in accordance with Luttinger's theorem.

In a previous publication[19], a diagrammatic scheme was proposed that uses the T–matrix formulation to derive an effective scattering potential which includes the effect of correlations as well as the bare scattering potential. As the first step of a systematic approach, we focus here on the one–particle effects of potential scattering in correlated systems by formulating a static ansatz using an unrestricted Slave-Boson (USB) method, which corresponds to the effective–medium renormalization of the scattering potential.

The calculations presented here are done for the slightly overdoped case, i.e. 17% doping away from half filling (i. e. the insulating case for the 2–D Hubbard model). In this case, we observe the $2k_F$–oscillations, essentially unrenormalized from the ones of the non–interacting case. Not only periodicity, but also the amplitude of the Friedel oscillations are shown here to be in excellent agreement with Quantum Monte Carlo (QMC) simulations. Corresponding calculations and comparisons with QMC for smaller doping are presently carried out, in order to test the simple effective medium approach also in the most interesting doping regime.

II. FORMALISM

We start with the Slave–Boson technique as formulated by Kotliar and Ruckenstein[20]. An elementary introduction to the Slave–Boson formalism for disorder–free applications can be found, for example, in the review articles by Arrigoni *et al.*[21] and Dieterich *et al.*[22]. The canonical transformation

$$c_{i\sigma}^\dagger \rightarrow (d_i^\dagger p_{i-\sigma} + p_{i\sigma}^\dagger e_i)f_{i\sigma}^\dagger \equiv \tilde{z}_{i\sigma}^\dagger f_{i\sigma}^\dagger, \qquad (1)$$

of the fermionic annihilation (creation) operator $c_{i\sigma}^{(\dagger)}$ introduces new bosonic operators $e_i^{(\dagger)}, p_{i\sigma}^{(\dagger)}, d_i^{(\dagger)}$ on a site i, which can be empty, singly occupied, or doubly occupied. Within the physical subspace the Hamiltonian can be written as

$$H_{SB} = -t \sum_{\substack{\langle i,j \rangle \\ \sigma}} \tilde{z}_{i\sigma}^\dagger f_{i\sigma}^\dagger f_{j\sigma} \tilde{z}_{j\sigma} + U \sum_i d_i^\dagger d_i + V_0 \sum_\sigma f_{0\sigma}^\dagger f_{0\sigma}. \qquad (2)$$

Here the impurity is modeled by a one–particle potential V_0 acting at the site $\vec{r} = 0$ of the lattice. This model can

be used, for example, to describe non–magnetic scatterers in high–T_c materials[23].

In the paramagnetic (spin–independent) saddle-point approximation of the path–integral, one calculates the partition function $\mathcal{Z}_{Stat} = e^{-S_{Stat}}$ by determing the stationary value of the effective action

$$S_{Stat} = -\text{Tr} \log \left[\delta_{ij}(\partial_\tau - \mu + V_0\delta_{i0} + \lambda_i^{(2)}) - t\, z_i z_j \right]$$
$$+ \beta \sum_i \{ d_i(\lambda_i^{(1)} - 2\lambda_i^{(2)} + U)d_i - \lambda_i^{(1)}$$
$$+ 2p_i(\lambda_i^{(1)} - \lambda_i^{(2)})p_i + e_i\lambda_i^{(1)}e_i \}, \tag{3}$$

which is given by the saddle–point equations, i. e.

$$\frac{\partial S_{Stat}}{\partial b_i} = 0, \quad b_i \in \{e_i, p_i, d_i, \lambda_i^{(1)}, \lambda_i^{(2)}\}. \tag{4}$$

The derivatives must be calculated with respect to all site–dependent bosonic variables and all Lagrange multipliers $\lambda_i^{(1/2)}$, which are introduced in order to restrict the enlarged, mixed bosonic-fermionic Hilbert space to the physical subspace within the functional integral[22]. Note that we use the standard renormalization factors $z_i = \frac{1}{\sqrt{1-d_i^2-p_i^2}}\tilde{z}_i\frac{1}{\sqrt{1-e_i^2-p_i^2}}$ in Eq. (3) to guarantee the correct $U \to 0$ limit[20]. On a 10×10 lattice and working at fixed average particle density n, one obtains 85 self–consistency equations by exploiting the spatial symmetry of the bosonic variables which are directly connected to physical observables. Within the Slave–Boson formalism, the particle density and the local magnetic moment are given by

$$n(\vec{r}_i) = 2d_i^2 + 2p_i^2, \tag{5}$$

and

$$m(\vec{r}_i) = 2p_i^2. \tag{6}$$

Compared to mean–field Slave–Boson approaches, which can be restricted to homogeneous, spiral or bipartite configurations, it takes considerably more numerical effort to find the extreme value of S_{Stat} in the high dimensional phase space encountered here. The strength of the Slave–Boson technique is that many–particle correlations are included via the z–factors in the effective masses of the quasi–free fermions. For the broken translational symmetry considered here, this renormalized mean–field method[24] also takes into account *site–dependent* hopping amplitudes $t_{ij}^{eff} = t\, z_i z_j$.

By examining the fermionic propagator G_f occurring in Eq. (3), one obtains the Dyson equation

$$G_f^{-1} = -[(\partial_\tau - \mu)\delta_{ij} - t\, z_i^* z_j] - (V_i\delta_{i0} + \lambda_i^{(2)})\delta_{ij}$$
$$= G_{0f}^{-1} - \Sigma^{USB}, \tag{7}$$

where the self energy is defined by

$$\Sigma^{USB} = (V_i\delta_{i0} + \lambda_i^{(2)})\delta_{ij}. \tag{8}$$

In an effective–medium or Hartree–like description of the scattering process one finds[19,25]

$$\Sigma^{Hartree} = (V_i\delta_{i0} + U\langle n_i\rangle)\delta_{ij}, \tag{9}$$

with site–dependent particle densities $\langle n_i\rangle$. Using the non–interacting propagator $G_{0f}^{-1} = -(\partial_\tau - \mu)\delta_{ij} - t\, z_i^* z_j$, Eq. (7) can be represented diagrammatically as in Fig. 1 (compare also to Fig. 1 of Ref. 17). Therefore, the correspondence of the Hartree– and the USB–method can be seen in the additional one–particle potential due to the interplay of correlations and disorder on the static "mean–field" level considered here.

III. RESULTS

In the past, the Slave–Boson method has been used as a powerful tool to calculate local quantities, which have turned out to be in excellent agreement with numerically exact results[24,26,27]. In order to check the reliability of the USB–method in the context of the extremely large system of coupled saddle–point equations, we compared our results to Quantum–Monte–Carlo calculations. The QMC–simulations suffer here from the problem of increasing numerical instability due to the broken translational symmetry, which limits the system size and the lowest accessible temperatures. Fig. 2 shows the comparison of the USB–data with QMC results for an 8×8–lattice. The charge density for $U = 4t$ (in the following, we set $t = 1$) is plotted as a function of the distance r/a from the impurity site, where a is the lattice constant. The saddle–point solution is almost identical to the QMC result despite the fact that the latter calculation is carried out at a relatively high temperature ($\beta = 6, T = 1/6$). Fig. 3 displays the USB oscillations of the charge density in the vicinity of the impurity at an inverse temperature $\beta = 100$ for various values of the correlation strength U. The solid line represents the non–interacting system and exhibits the well–known $2k_F$–oscillations, corresponding here to a wavelength of $\lambda \approx 1.5a$. While the $2k_F$–periodicity is unaffected[29], repulsive interactions diminish the amplitude of the Friedel oscillations. They lead for strong correlations ($U > 10$) eventually to a short–range, monotonically decaying behavior. The reason for this is that for increasing U the renormalized (pseudo–fermionic) particles with correlation–enhanced effective masses become more and more ineffective in contributing to screening processes. For attractive interactions, the impurity locally breaks particle–hole symmetry and causes large Friedel amplitudes. This is due to the tendency of the attractive Hubbard model to form a charge–density–wave instability, which occurs in the unperturbed system at half–filling[30,31]. The oscillations present at $r/a > 5$ are due to interference effects at the corners of the 10×10 lattice. They are irrelevant for, for

example, averaged random impurity sites.

Fig. 4 exhibits the influence of the potential strength V_0 on the corresponding charge density behavior. Increasingly attractive impurities enhance the amplitude until the maximum density ($n \to 2$) is reached at the impurity site $r = 0$ (inset of Fig. 4). Stronger potentials decrease the energy of the bound states below the quasi-particle band. A symmetric repulsive–attractive effect of the impurity can be found in the oscillations for $V_0 = \pm 1$ around the average density ($n = 0.81$). Further USB–calculations showed that higher temperatures cause a decrease of Friedel oscillations, which is in accordance with the smearing out of the jump in the Fermi function at k_F, which determines, for example, the integral bond in a continuum calculation[32] of $n(r)$. This is also the origin of the moderate oscillations in Fig. 2 at $\beta = 6$. We note that no significant deviations from the above described behavior were found in the investigated metallic phase at $0.7 < n < 0.9$.

We now concentrate on the one–particle spectra obtained from the USB–calculations. Using the pseudo–fermionic propagator, we obtain the density of states

$$D(\omega) = -\frac{1}{N\pi} \sum_m \operatorname{Im} G_f(m, \omega + i\eta),$$
$$= \frac{1}{N} \sum_m \delta(\omega - \varepsilon_m). \tag{10}$$

This function, with the δ–functions replaced by η–broadened functions, is plotted in Fig. 5. The broken translational symmetry lifts the degeneracy of various quasi-particle states of the unperturbed system (solid line) and produces a single bound state (arrow in Fig. 5) separated from the band. Note that this band has a smaller width than in the non–interacting case due to the Slave–Boson renormalization effects. The bound state possesses s–wave symmetry (see, for example, the first state in Fig. 6), as does the bare scattering potential V_0. Therefore, within our static potential renormalization[25], the effective impurity potential[19] is not strong enough to cause the previously proposed (and verified in numerical simulations[33]) anisotropic scattering processes, resulting, for example in bound states of higher symmetries. These extended bound states can be found by introducing an additional bare one–particle potential V_1 at the neighboring sites, which produces states of all the possible irreducible representations[19]. Fig. 6 shows the corresponding amplitudes of the pseudo–fermionic (bound state) wave-functions $|\Psi_m\rangle = \sum_i c_{mi} f_i^\dagger |vac\rangle$, belonging to the six lowest lying energies ε_m.

Another interesting feature, found in the USB–results, occurs in the magnetic structure influenced by the non–magnetic impurity. We first investigate the local magnetic moment $m(0)$ at the impurity site $\vec{r} = 0$. In Fig. 7, this quantity is plotted (for fixed U and average particle density n) as a function of the potential strength V_0 and the corresponding local particle density $n(0)$. The maximum of $m(0)$ at $V_0 \approx -1.0$ corresponds to a locally

half–filled impurity site, i. e. $n(0) = 1$, and signals the formation of a magnetic state. This situation is analogous to the mean–field description of the Single–Impurity Anderson model and was also found in exact diagonalization studies of a Hubbard chain containing a single impurity by Hallberg and Balseiro[35]. In order to evaluate the size of the magnetic moment, one should perform spin–dependent USB–calculations, which could then also be extended to the symmetry–broken phases found near half–filling[24,27]. The paramagnetic subspace to which we restrict the solution appears sufficient for the questions investigated here. Substituting $U + U_0$ for the local interaction strength U at $\vec{r} = 0$, one shifts the magnetic transition point by a small U_0, which can be seen in the inset of Fig. 7. This means that the appearance of a magnetic state depends on a fine tuning of the system parameters, which could be one reason for the experimental disagreement concerning the size and existence of a magnetic moment[9-15]. Strong potentials eventually lead to the formation of a $S = 0$ spin–singlet (in the limit of no or double occupancy), which corresponds in Fig. 7 to a minimal local moment at the impurity site. Interestingly, the oscillations of the charge density are also accompanied by spatial variations of the magnetic moment. Using the parameters relevant for Fig. 7, Fig. 8 shows the magnetic structure in the vicinity of the impurity. For $V_0 = -1$, the magnetic state at $\vec{r} = 0$ produces a relatively small amplitudes $m(r)$. The stronger attractive potential, $V_0 = -4$, creates a singlet bound state at $\vec{r} = 0$ and leads to a maximal moment at a distance of $r = \sqrt{2}$. This can be connected to the experimentally detected spatially extended (para–)magnetic moments around Zn–impurities. In a theoretical picture, this feature of the metallic phase can be seen as a reminiscence of correlation–induced bound states, carrying localized magnetic moments, at half–filling[33,34].

IV. CONCLUSION

In summary, we have extended the Slave–Boson mean–field method to systems with a spatially inhomogeneous phase space. This technique can be used to calculate single–particle properties of correlated–lattice models which include a non–magnetic impurity. Formally, this method corresponds to a static renormalization of the impurity potential in analogy to a diagrammatic effective–medium Hartree approach to impurity scattering[19].

We have solved numerically the complicated system of 85 coupled saddle–point equations for a 10×10 Hubbard model in the metallic phase. The USB–results show, in accordance with QMC–data, Friedel oscillations of the charge density in the vicinity of the impurity. The amplitude is reduced by repulsive correlations, while the attractive system display a charge–density–wave enhancement. The system parameters can be chosen, so that a magnetic state appears at the impurity site, signaled

by the maximal local magnetic moment. In addition, the range of the magnetic correlations around the impurity increases with increasing potential strength, being in qualitative accordance with experimental results.

The above formalism and its results can be viewed as the first step of a systematic investigation of correlation effects on impurity scattering. Higher diagrammatic orders of many–body interactions will be studied in a future publication[25].

[1] P. J. Hirschfeld, P. Wölfle and D. Einzel, Phys. Rev. B **37**, 83 (1988).

[2] T. Hotta, J. Phys. Soc. Jpn. **62**, 274 (1993).

[3] L. S. Borkowski and P. J. Hirschfeld, Phys. Rev. B **49**, 15404 (1994).

[4] R. Fehrenbacher and M. R. Norman, Phys. Rev. B **50**, 3445 (1994).

[5] S. M. Quinlan and D. J. Scalapino, Phys. Rev. B **51**, 497 (1994).

[6] P. J. Hirschfeld, W. O. Puttika and D. J. Scalapino, Phys. Rev. B **50**, 10250 (1994).

[7] T. Xiang and J. M. Wheatley, Phys. Rev. B **51**, 11721 (1995).

[8] D. J. Scalapino, Phys. Rep. **250**, 329 (1995).

[9] G. Xiao *et al.* , Phys. Rev. B **42**, 8752 (1990).

[10] A. V. Mahajan *et al.* , Phys. Rev. Lett. **72**, 3100 (1994).

[11] A. M. Finkel'stein *et al.* , Physica C **168**, 370 (1990).

[12] H. Alloul *et al.* , Phys. Rev. Lett. **67**, 3140 (1991).

[13] R. E. Walstedt *et al.* , Phys. Rev. B, **48**, 10646 (1993).

[14] M. Z. Cieplak *et al.* , Phys. Rev. B **46**, 5536 (1992).

[15] K. Ishida *et al.* , J. Phys. Soc. Jpn. **62**(8), 2803 (1993).

[16] P. Mendels *et al.* , Phys. Rev. B **49**, 10035 (1994).

[17] Z.–X. Shen and D. S. Dessau, Phys. Rep. **253**, 1 (1995).

[18] H. Ding *et al.* , Phys. Rev. Lett. 76, 533 (1996).

[19] W. Ziegler, D. Poilblanc, R. Preuss, W. Hanke and D. J. Scalapino, Phys. Rev. B **53**, 8794 (1996).

[20] G. Kotliar and A. E. Ruckenstein, Phys. Rev. Lett. **57**, 1362 (1986).

[21] E. Arrigoni, C. Castellani, M. Grilli, R. Raimondi and G. C. Strinati, Phys. Rep. **241**, 291 (1994)

[22] P. Dieterich, W. Ziegler, A. Muramatsu and W. Hanke, to appear in Phys. Rep. (1997).

[23] R. Fehrenbacher, Phys. Rev. Lett. **77**, 1849 (1996).

[24] L. Lilly, A. Muramatsu and W. Hanke, Phys. Rev. Lett. **65**, 1379 (1990).

[25] W. Ziegler, G. Hildebrand and W. Hanke, to be published.

[26] R. Frésard and P. Wölfle, J. Phys. Cond. Mat. **4**, 3625 (1992).

[27] W. Ziegler, P. Dieterich, A. Muramatsu and W. Hanke, Phys. Rev. B **53**, 1231 (1996).

[28] R. Preuss, A. Muramatsu, W. von der Linden, P. Dieterich, F. F. Assaad and W. Hanke, Phys. Rev. Lett. **73**, 732 (1994).

[29] The anisotropic Fermi–surface of the lattice system causes the small deviations from a harmonic oscillation in Fig. 3.

[30] L. Lilly, A. Muramatsu and W. Hanke, Phys. B **165**& **166**, 393 (1990).

[31] A. Moreo and D. J. Scalapino, Phys. Rev. Lett. **66**, 949 (1991).

[32] G. D. Mahan, *Many particle physics*, 2nd ed., Plenum Press, New York (1990).

[33] D. Poilblanc, D. J. Scalapino and W. Hanke, Phys. Rev. Lett. **72**, 884 (1994).

[34] D. Poilblanc, D. J. Scalapino and W. Hanke, Phys. Rev. B **50**, 13020 (1994).

[35] K. A. Hallberg and C. A. Balseiro, Phys. Rev. B **52**, 374 (1995).

Figure captions

FIG. 1: Diagrammatic representation of the self–consistent pseudo–fermionic one–particle propagator G_f (double line). The scattering by the impurity is depicted by the cross, the zig–zag line represents the Slave–Boson self–energy, i. e. the Lagrange parameter $\lambda^{(2)}$.

FIG. 2: Radial modification of the charge density caused by a δ–potential $V_0 = -8.0$ The data points of the Slave-Boson calculation fit the QMC–distribution for the Hubbard–model at $U = 4$, $\beta = 6$ and an average density $n = 0.83$.

FIG. 3: Correlations effects on the low–temperature ($\beta = 100$) Friedel oscillations induced by a δ–potential of strength $V_0 = -4.0$.

FIG. 4: USB–calculations for different impurity potentials in the Hubbard model ($U = 4$, $\beta = 100$). Repulsive (attractive) interactions reduce (enhance) the amplitude of Friedel oscillations.

FIG. 5: USB–spectra of the pseudo–fermionic propagator. The density of states shows an impurity–induced s–wave bound–state below the renormalized quasi-particle band. The broken translational symmetry creates states between the unperturbed ($V_0 = 0$) single–particle energy levels.

FIG. 6: Wave functions of the six lowest pseudo–fermionic eigenstates caused by an extended impurity ($V_0 = -8.0$, $V_1 = -4.8$). The wave functions exhibit s–, $p_{x/y}$– (degenerated), s–, $d_{x^2-y^2}$– and s–wave symmetry, in order from upper left to lower right.

FIG. 7: Charge density and magnetic moment at the impurity site ($r = 0$). The scattering potential acts in the $U = 4$ Hubbard model at $\beta = 100$. The maximum of $m(0)$ and the half–filled site displays the formation of a magnetic state.

FIG. 8: The local magnetic moment in the vicinity of the impurity. The spatial magnetic distribution and its maximum depends on the strength of the scattering potential V_0.
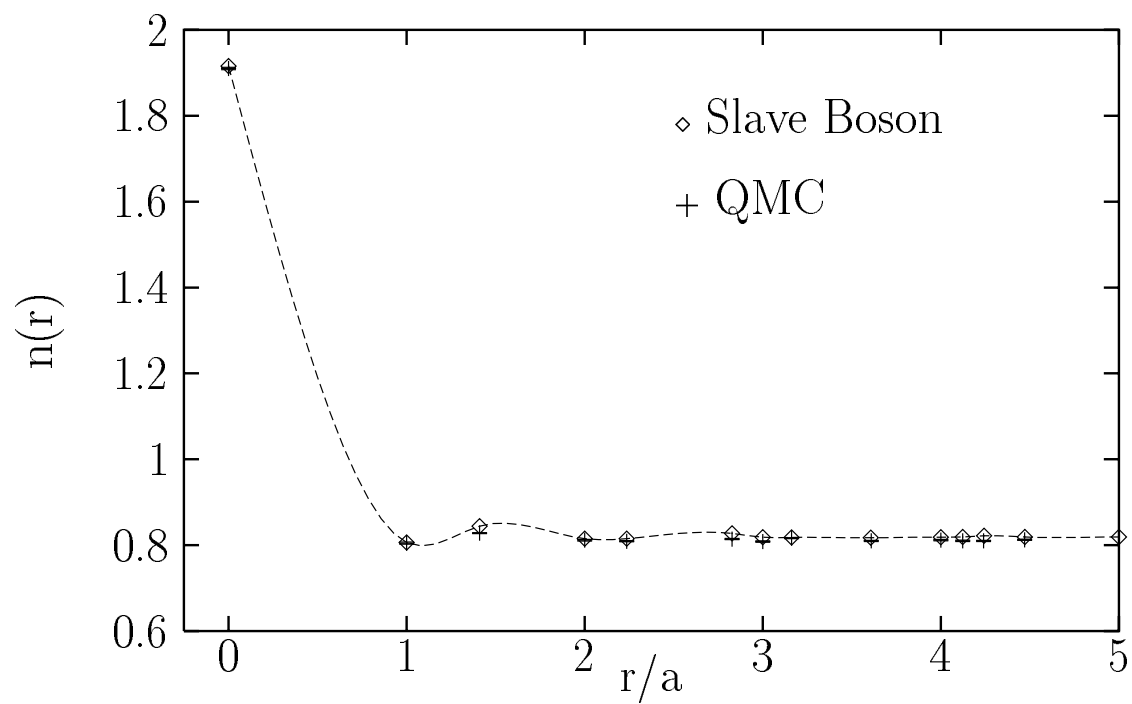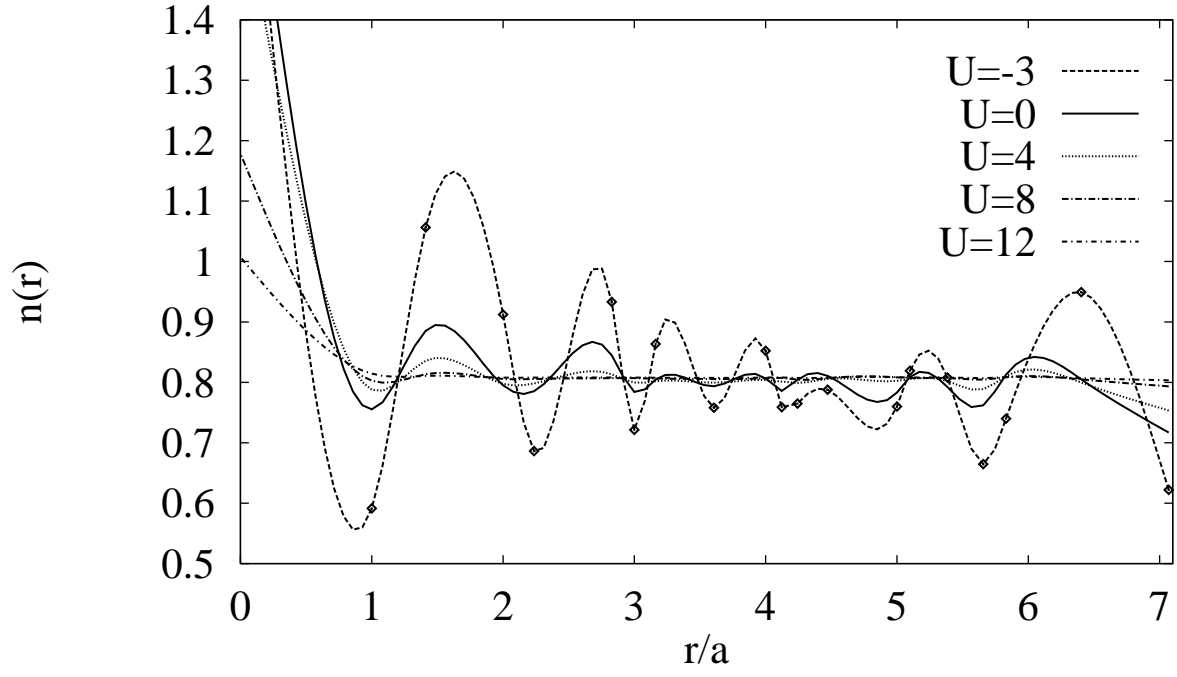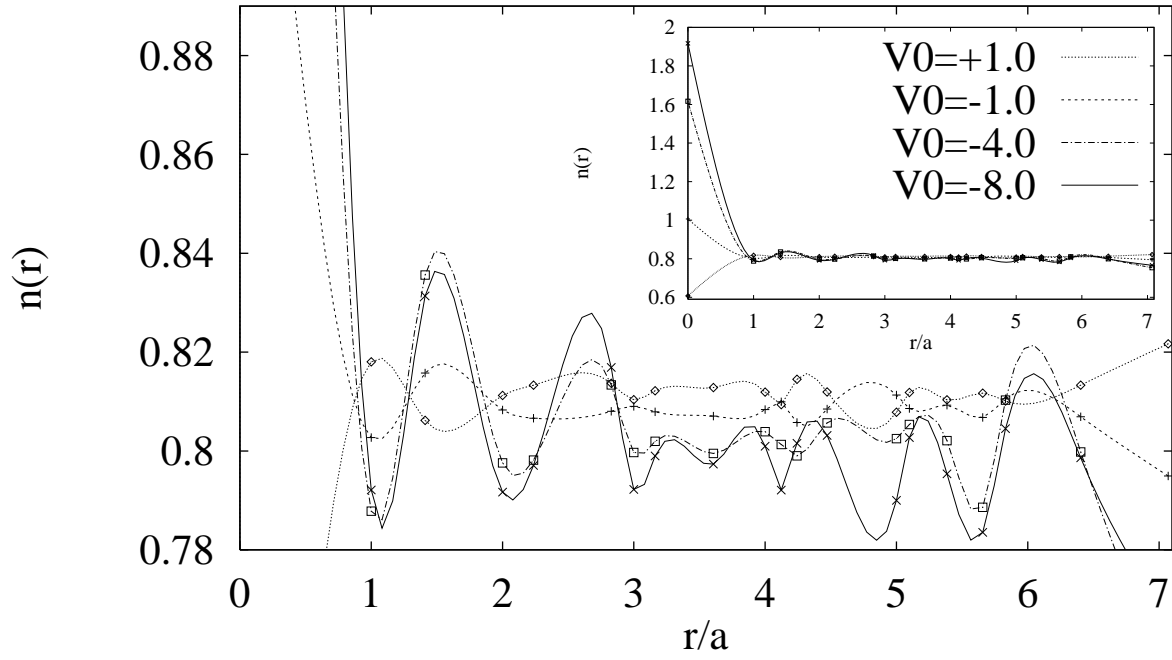
FIG. 1

FIG. 2

FIG. 3

FIG. 4

FIG. 5

FIG. 6

FIG. 7

FIG. 8